SANDIA REPORT
SAND78-0577 • Unlimited Release • UC-60

Printed April 1978

Torque Ripple in a Vertical Axis Wind Turbine

Robert C. Reuter, Mark H. Worstell

Prepared by
Sandia National Laboratories
Albuquerque, New Mexico 87185 and Livermore, California 94550
for the United States Department of Energy
under Contract DE-AC04-76DP00789

SF2900Q(8-81)

Printed in the United States of America
Available from
National Technical Information Service
U.S. Department of Commerce
5285 Port Royal Road
Springfield, VA 22161

NTIS price codes
Printed copy: A03
Microfiche copy: A01

SAND78-0577

TORQUE RIPPLE IN A VERTICAL AXIS WIND TURBINE

Robert C. Reuter, Jr.*

and

Mark H. Worstell†

ABSTRACT

Torque ripple is a name given to time variations in torque which are propagated through the drive train of wind energy conversion systems. This paper covers an analytical and experimental investigation of torque ripple in a Darrieus vertical axis wind turbine. An analytical model of the turbine is described and numerical results from a solution to the equations of this model are compared to experimental results obtained from the existing DOE/Sandia 17 meter vertical axis wind turbine. Discussions on the sources of torque ripple, theoretical and experimental correlation, and means of suppressing its magnitude are included.

*Applied Mechanics Division III, 1284

†Advanced Energy Projects Division, 5715

NOMENCLATURE

D	Induction generator damping coefficient
f	Ratio of power loss to mean power input
$J_1 = J_2$	Half the polar moment of inertia of the blades
J_3, J_4	Polar moments of inertia of transmission and generator, respectively
k	Synchronous generator stiffness
K_1	Rotor shaft stiffness
K_2	Low speed shaft stiffness
K_3, K_4	High speed shaft stiffness as seen by transmission and generator, respectively
K_I	Intermediate speed shaft stiffness (uncorrected for speed)
K_H	High speed shaft stiffness (uncorrected for speed)
M_T	Torque ripple magnification factor
n_1, n_2	Gear ratios of the transmission and belt drive, respectively
R_{max}	Maximum turbine radius
t	Time
$\tilde{T}$	Torque ripple
T_{A1}, T_{A2}	Applied aerodynamic torques at top and bottom blade attachment points, respectively
T_1, T_2	Periodic components of applied torques
T_{GI}, T_{GS}	Induction and synchronous generator reactions, respectively
V_∞	Freestream wind speed
θ_i	Angular displacement
λ	Tip speed ratio
τ_1, τ_2	Mean values of applied torques
ω	Excitation frequency

ω_s Synchronous generator speed

ω_{Ti} Local shaft speed

Ω Turbine operating speed

INTRODUCTION

An intrinsic, mechanical phenomenon associated with the operation of wind energy conversion systems is called "torque ripple". Torque ripple is a name given to the time variations in torque which are transmitted through the various components of a wind turbine drive train ultimately to its load. Under the most ideal conditions of a steady wind from a fixed direction, torque ripple in a horizontal axis wind turbine is caused by wind shear and tower shadow (1) and in a vertical axis wind turbine by continuously changing angles of attack between the apparent wind and the turbine blades (2,3). Other events which contribute to the development of torque ripple include variations in wind magnitude and direction, blade dynamics, blade stall and torsional slack in the drive train. If sufficiently large, torque ripple may have a detrimental effect on fatigue life of various drive train components (such as shafts, couplings and transmissions) and on output power quality. It may also cause the generator pull-out torque to be exceeded, resulting in a sudden loss of load and possible turbine run-away. Torque ripple is clearly a concern of both horizontal and vertical axis wind turbine proponents, and deserves the attention of detailed investigations.

Based on a set of specific assumptions (delineated below) this paper summarizes the major portion of a theoretical and experimental study of the torque ripple phenomenon in Darrieus vertical axis wind turbines in a synchronous, or near synchronous, power grid application. The paper covers development of a lumped mass model of the turbine and its drive train components, an analytical solution for torque ripple based on the model, a discussion of torque ripple data collection and reduction, a comparison of theory and experiment, and a discussion of the phenomenon with a view toward reducing its magnitude. The experimental data were obtained from the DOE/Sandia 17 meter turbine (in its 2 bladed configuration) presently located in Albuquerque, New Mexico.

DRIVE TRAIN DESCRIPTION AND MODEL

The drive train of a typical wind energy conversion system has basic components consisting of the rotor, the low speed shaft, the transmission, the high speed shaft and finally the generator. In the case of the vertical axis turbine, the rotor consists of the blades and a turbine rotor shaft to which the blades are attached. This rotor shaft must be sufficiently strong to carry torque and loads from aloft, and sufficiently stiff to prevent excessive lead-lag blade motion or dynamic resonance (4).

The drive train of the DOE/Sandia 17 meter wind turbine is represented in Fig. 1. The turbine rotor shaft is supported by four guy cables at the top with tapered roller bearings, top and bottom, supporting the loads of the rotor and guy cables. Two disc brakes, one used as the normal brake and the other as an emergency brake, are located on the turbine rotor shaft above the bottom rotor shaft bearing. Two flexible couplings, composed of rubber shear sandwich mountings, are located on the low speed shaft just above the transmission. These couplings provide shaft misalignment accommodation, flexibility of testing various drive train stiffnesses, and mechanical shock protection of the torque sensor that is placed between the couplings.

The transmission is a vertically mounted, three stage planetary gearbox with an overall ratio of 42.87:1. A dry sump lubrication system was incorporated in order to reduce viscous losses. A right angle gearbox with a ratio of 1:1 provides a horizontal take off directly beneath the planetary gearbox. Synchronous turbine speed changing capability is accomplished by a timing belt and pulley arrangement downstream from the right angle gearbox. By changing the sizes of the pulleys, 13 discrete synchronous turbine speeds from 29.6 RPM to 59.5 RPM are available. Specifically, the ratio of the belt drive can vary from 1.42:1 to .71:1. Thus, the high speed end of this turbine consists of two stages, one on

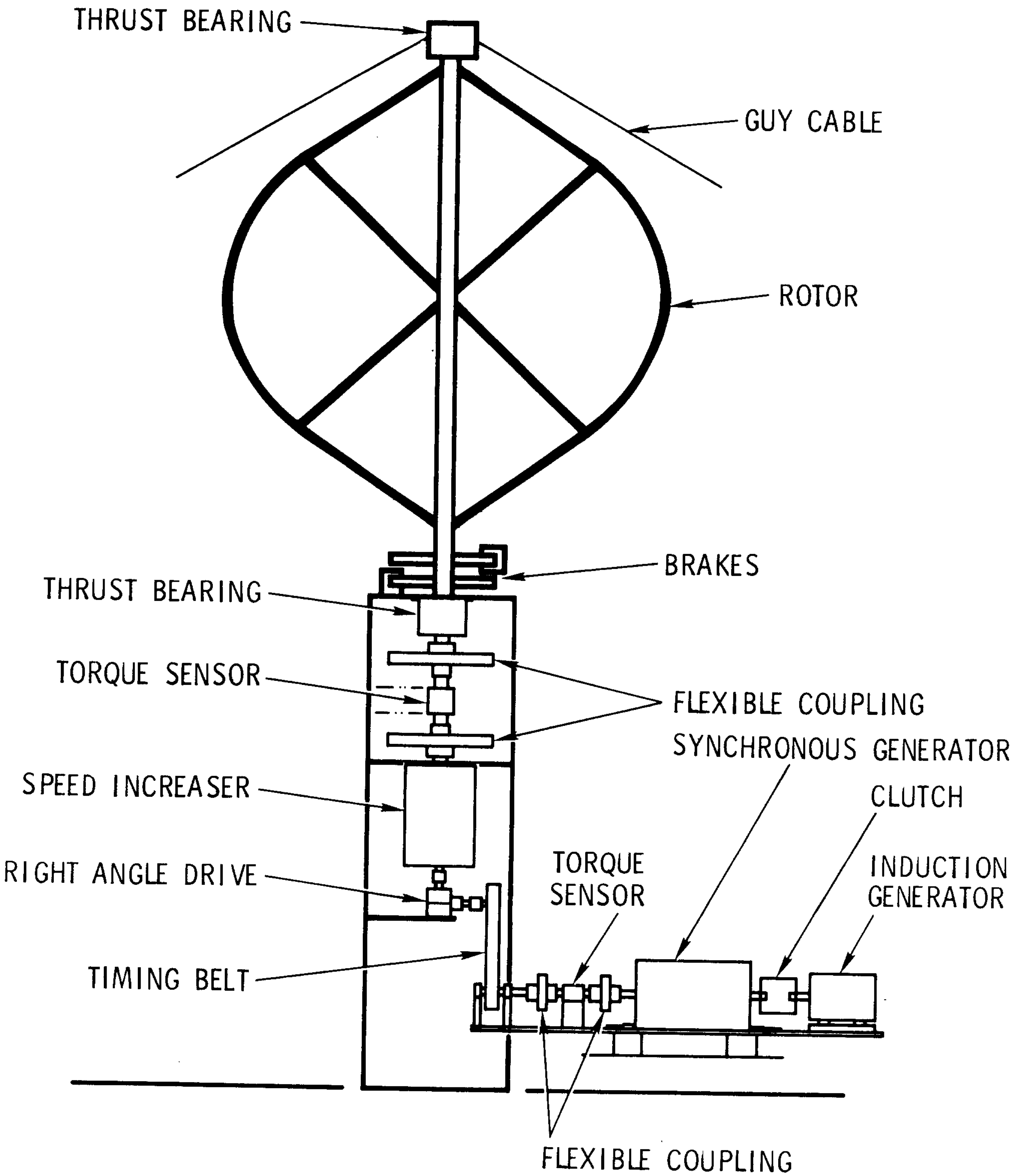

Fig. 1 - Schematic of DOE/Sandia 17 meter vertical axis wind turbine and drive train

either side of the belt drive. Another set of flexible couplings, isolating a second torque sensor, is located on the output shaft of the belt drive, or high speed shaft, just upstream of the generators.

The 17 meter turbine has two generator/motors coupled in tandem by an electric clutch on the high speed end of the drive train. One is a synchronous generator and the other is an induction generator. Either one of these machines can function as a generator or a motor, depending on the torque direction of the turbine output shaft. The synchronous generator operates at a constant 1800 RPM while the induction generator will experience a 3% slip in speed from 1800 RPM at the rating. Both generators are rated at 60 KW and are 480 volt three phase. The induction generator is used to bring the turbine up to speed because of its better starting characteristics. The incorporation of both generators affords flexibility in the evaluation of synchronous and induction power generation.

A mathematical model for the 17 meter turbine is depicted in Fig. 2. The turbine rotor inertia is modeled by two disks, J_1 and J_2, with a torsional spring, K_1, in between. Each of these disks represents $\frac{1}{2}$ the actual turbine rotor inertia while K_1 is the torsional stiffness of the turbine rotor shaft. The aerodynamic torque input to the turbine rotor is represented by T_{A1} and T_{A2} and acts upon the rotor disks. T_{A1} and T_{A2} are written with different coefficients to account for wind shear if desired (e.g., the top half of the turbine rotor produces more torque than the lower half).

The torsional stiffness of the low speed end of the drive train, between the bottom of the turbine rotor and the top of the planetary gearbox, is represented by K_2. By removing half of the shear mountings in each flexible coupling along this shaft, it is possible to reduce K_2 by 43%, thus "softening" the low speed end. The inertia of the planetary gearbox was calculated relative to the low speed end and is given by J_3. The planetary gearbox speed increase ratio is

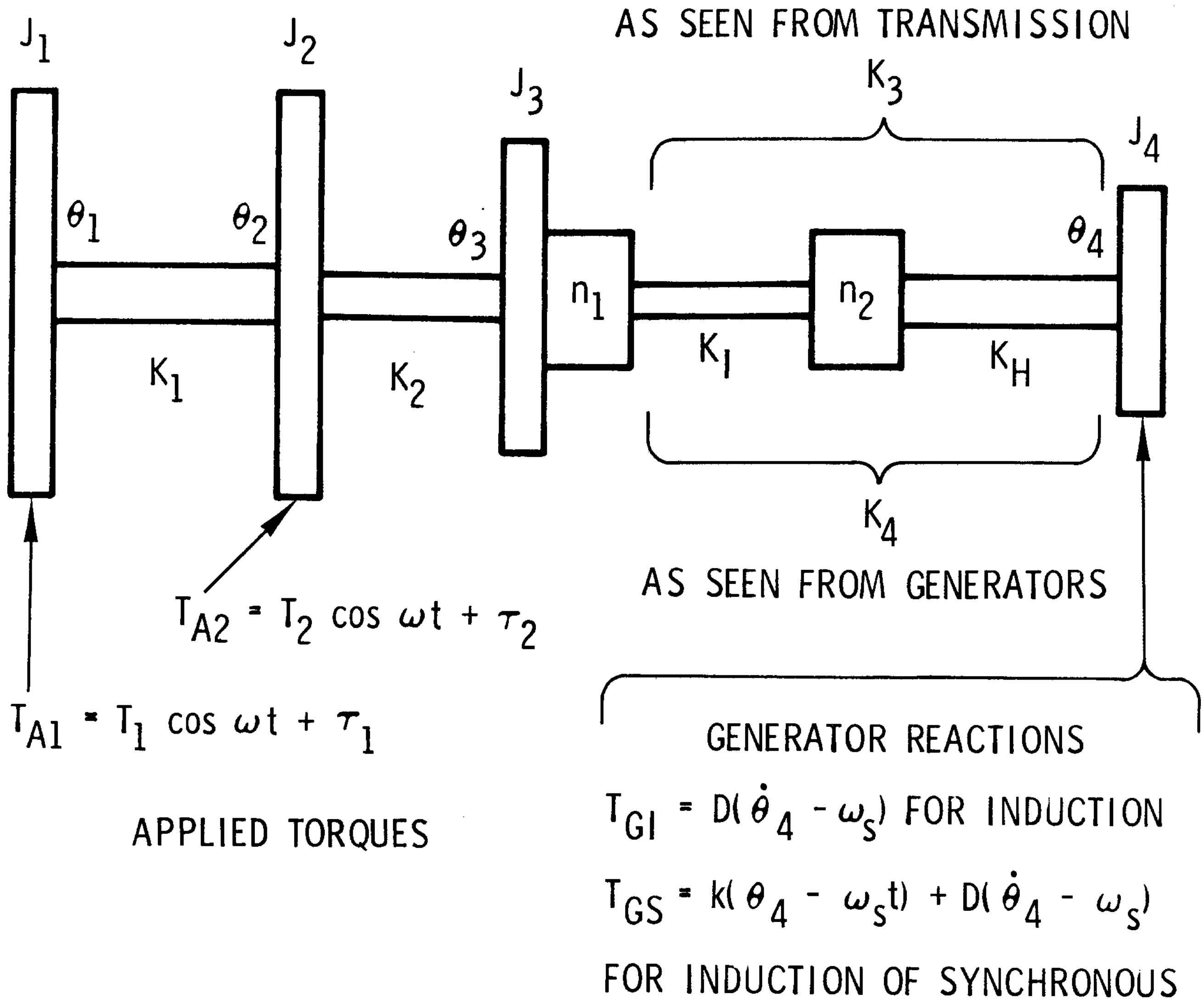

Fig. 2 - Schematic of turbine and drive train components for analytical model

represented by n_1. The torsional stiffnesses of the drive shafts from the bottom of the planetary gearbox to the pulleys and the equivalent torsional stiffness of the timing belt are included in K_I. This portion is the first stage of the high speed end. The gear ratio of the belt drive is n_2. Finally, K_H is the torsional stiffness of the second stage of the high speed end of the drive train, between the pulleys and the generators. K_3 and K_4 are equivalent high speed shaft stiffnesses referred to the low and high speed ends, respectively, and are expressed in terms of n_1, n_2, K_I and K_H; see Table I.

The combined inertia of both generators and the clutch is given by J_4. The applied torque on this disk is the torque reaction of the generators. T_{GI} is the torque of the induction motor while T_{GS} is the combined torque of both the synchronous and induction generators. In all testing performed, the clutch between the generators was continually engaged. When using the induction generator only, the field in the synchronous generator was left unexcited to eliminate its torque reaction. When the synchronous generator is brought on line, the average speed of the high speed end becomes a synchronous 1800 RPM at which the induction generator torque vanishes. Due to the nature of the synchronous generator, however, there are instantaneous changes from the synchronous speed even though the average is still 1800 RPM. Because of this, the induction motor torque is included in T_{GS}.

The values for all the inertias, torsional stiffnesses, gear ratios, and generator coefficients of the 17 meter turbine model are listed in Table I.

ANALYSIS

Because of the analytical complexities introduced by attempting to take into account all events which contribute to the development of torque ripple, several simplifying assumptions were made. Thus, an initial understanding of

TABLE I. Turbine Properties for Model

$J_1 = J_2 = 9.83 \times 10^4$ lb-sec^2-in (1.11×10^4 N-sec^2-m)

$J_3 = 2.15 \times 10^3$ lb-sec^2-in (2.43×10^2 N-sec^2-m)

$J_4 = 25.7$ lb-sec^2-in (2.90 N-sec^2-m)

$K_1 = 9.82 \times 10^7$ lb-in/rad (1.11 N-m/rad)

$K_2 = 3.97 \times 10^6$ lb-in/rad (4.49×10^5 N-m/rad) (stiff)

$K_2 = 2.27 \times 10^6$ lb-in/rad (2.56×10^5 N-m/rad) (soft)

$K_I = 1.25 \times 10^6$ lb-in/rad (1.41×10^5 N-m/rad)

$K_H = 3.36 \times 10^4$ lb-in/rad (3.80×10^3 N-m/rad)

(5) $$K_3 = \frac{n_1^2 n_2^2 K_I K_H}{K_I + n_2^2 K_H}$$

(6) $$K_4 = \frac{K_I K_H}{K_I + n_2^2 K_H}$$

$n_1 = 42.87$

Turbine RPM	29.6	37.0	45.5	52.5
n_2	1.416	1.134	.923	.800

$D = 510.0$ lb-in-sec/rad (57.6 N-m-sec/rad)

$k = 1.13 \times 10^4$ lb-in/rad (1.27×10^3 N-m/rad)

$\omega_s = 188.5$ rad/sec

the phenomenon and identification of important parameters is possible. These assumptions are:

1. The wind is steady, uniform and from a fixed direction.
2. Blade stall does not occur.
3. Drive train slack does not exist.
4. Spacially distributed inertias of the drive train shafts and couplings are small in comparison to the concentrated inertias of the blades, transmission and generator.
5. Total blade inertia may be divided and lumped.
6. Generator response is linear.
7. Turbine and drive train response is linear elastic.
8. There are no mechanical or aerodynamic losses in the system.
9. Blade frequencies are above the turbine operating speeds.

The assumption of a steady, uniform and fixed direction wind is perhaps one of the most disputable made. It can be accommodated, however, by using some discretion in selecting data for comparison with the theory (this will be expanded upon later). If a blade stalls at any azimuth position, aerodynamic lead-lag (chordwise) forces become non-harmonic, resulting in the necessity of a complex analytical characterization (5). To avoid this complication, only tip speed (at the maximum radius) to wind speed ratios, $\lambda (= R_{max} \Omega / V_{\infty})$, greater than or equal to 4 are considered, and the analytical solution remains harmonic. Another weak assumption is that no power losses occur in the system. Over a year of operating experience with the DOE/Sandia 17 meter turbine has demonstrated that significant losses do occur, principally in the transmission. The effect of power loss on torque ripple will be discussed later.

In spite of the above assumptions, the analytical model is flexible enough to include several important generalities. The model includes a wide range of parameters so that a large spectrum of turbine designs can be evaluated. These parameters include blade, transmission and generator rotational inertias, torsional rigidities of all rotating shafts, couplings and belts in the drive train, response properties of either induction or synchronous generators, and two speed changes separated by flexible shafts. In addition, applied loads can permit the characterization of wind shear. The model is general and accurate enough to perform parameter studies with relative ease.

For the purposes of this paper, torque ripple is defined as a harmonic oscillation of torque about some mean value. Its magnitude is given by

$$\tilde{T} = \frac{T_{max} - T_{mean}}{T_{mean}} \tag{1}$$

By this definition, a torque oscillation about a zero mean yields an infinite torque ripple, and a steady torque yields zero torque ripple.

Without going into great detail, the analytical solution is as follows. Equilibrium requires that the succeeding equations be satisfied.

$$\left.\begin{aligned}
&J_1\ddot{\theta}_1 + K_1(\theta_1 - \theta_2) = T_{A1} \\
&J_2\ddot{\theta}_2 + K_2(\theta_2 - \theta_3) + K_1(\theta_2 - \theta_1) = T_{A2} \\
&J_3\ddot{\theta}_3 + K_3\left(\theta_3 - \frac{\theta_4}{n_1 n_2}\right) + K_2(\theta_3 - \theta_2) = 0 \\
&J_4\ddot{\theta}_4 + K_4(\theta_4 - n_1 n_2 \theta_3) + D(\dot{\theta}_4 - \omega_s) = 0 \\
&\text{where } K_4 = \frac{K_3}{(n_1 n_2)^2}
\end{aligned}\right\} \tag{2}$$

Strictly speaking, the form of the last of Eq. (2) represents the response of an induction generator (see Fig. 2). The addition of a synchronous generator may be characterized simply by including k (see Fig. 2) in series with K_4.

Solutions of Eq. (2) are of the form

$$\theta_i = R_i \cos(\omega t - \alpha_i) + \omega_{Ti} t + C_i, \qquad i = 1,2,3,4 \tag{3}$$

where C_i is an initial condition constant which can be ignored here without loss of generality, and α_i is a phase angle. Also, ω is the circular frequency of the lead-lag forcing function with is 2/rev (twice the turbine speed) for a two bladed turbine and 6/rev for a three bladed turbine (2). Substitution of (3) into (2) yields

$$\left.\begin{aligned}
\phi_1 B_1 - K_1 B_2 &= T_1 \\
\phi_1 A_1 - K_1 A_2 &= 0 \\
\phi_2 B_2 - K_1 B_1 - K_2 B_3 &= T_2 \\
\phi_2 A_2 - K_1 A_1 - K_2 A_3 &= 0 \\
\phi_3 B_3 - K_2 B_2 - \frac{K_3}{n_1 n_2} B_4 &= 0 \\
\phi_3 A_3 - K_2 A_2 - \frac{K_3}{n_1 n_2} A_4 &= 0 \\
\phi_4 B_4 - n_1 n_2 K_4 B_3 &= -\omega D A_4 \\
\phi_4 A_4 - n_1 n_2 K_4 A_3 &= \omega D B_4
\end{aligned}\right\} \tag{4}$$

where

$$\left.\begin{array}{lll}\phi_1 = (K_1 - \omega^2 J_1) & , & \phi_2 = (K_1 + K_2 - \omega^2 J_2) \\ \phi_3 = (K_2 + K_3 - \omega^2 J_3) & , & \phi_4 = (K_4 - \omega^2 J_4)\end{array}\right\} \quad (5)$$

and

$$A_i = R_i \sin \alpha_i, \qquad B_i = R_i \cos \alpha_i, \qquad i = 1,2,3,4 \qquad (6)$$

The next step is to solve Eq. (4) for the A_i's and B_i's. This may be done numerically, with the aid of a computer, or algebraically, using a computer only for numerical evaluation of final expressions. The latter method was used in this investigation. In as brief a form as possible, the following expressions were found for the unknown constants. These expressions will be called Eq. (7).

$$A_1 = \frac{\omega D K_2^2 K_3 K_4 \left[\phi_1(\phi_2\ T_1 + K_1 T_2) - T_1(\phi_1\phi_2 - K_1^2)\right]}{\left[\left\{\phi_4\left[\phi_3(\phi_1\phi_2 - K_1^2) - \phi_1 K_2^2\right] - K_3 K_4(\phi_1\phi_2 - K_1^2)\right\}\left[(\phi_3\phi_4 - K_3K_4)(\phi_1\phi_2 - K_1^2) - \phi_1\phi_4 K_2^2\right] + (\omega D)^2\left[\phi_3(\phi_1\phi_2 - K_1^2) - \phi_1 K_2^2\right]^2\right]}$$

$$B_1 = \frac{\left\{-\omega D\left[\phi_3(\phi_1\phi_2 - K_1^2) - \phi_1 K_2^2\right]A_1 - \phi_4\left[K_2^2 T_1 - \phi_3(\phi_2 T_1 + K_1 T_2)\right] - K_3K_4(\phi_2 T_1 + K_1 T_2)\right\}}{\left\{\phi_4\left[\phi_3\ (\phi_1\phi_2 - K_1^2) - \phi_1 K_2^2\right] - K_3 K_4(\phi_1\phi_2 - K_1^2)\right\}}$$

$$A_2 = \frac{\phi_1}{K_1} A_1 \qquad , \qquad A_3 = \frac{(\phi_1\phi_2 - K_1^2)}{K_1 K_2} A_1$$

(Eq. 7 continued:)

$$A_4 = \frac{n_1 n_2}{K_1 K_2 K_3} \left[\phi_3(\phi_1\phi_2 - K_1^2) - \phi_1 K_2^2\right] \quad A_1$$

$$B_2 = \frac{\phi_1}{K_1} B_1 - \frac{T_1}{K_1} \quad , \quad B_3 = \frac{(\phi_1\phi_2 - K_1^2)}{K_1 K_2} B_2 - \frac{(\phi_2 T_1 + K_1 T_2)}{K_1 K_2}$$

$$B_4 = \frac{n_1 n_2}{\omega D K_1 K_2 K_3} \left[(\phi_3\phi_4 - K_3 K_4)(\phi_1\phi_2 - K_1^2) - \phi_1\phi_4 K_2^2\right] \quad A_1$$

This completes the basic formulation of the solution. Amplitudes and phase angles are obtained from Eq. (6) as

$$R_i = (A_i^2 + B_i^2)^{\frac{1}{2}}$$

$$\alpha_i = \tan^{-1} \frac{A_i}{B_i}$$

Torque (and therefore torque ripple) at any location along the drive train can be calculated from the above. Torque data were obtained at two locations in the DOE/ Sandia 17 meter turbine, the low speed and the high speed shafts. Expressions for torque at these two locations are given by

$$T_L = K_2(\theta_2 - \theta_3) \text{ and } T_H = K_4(n_1 n_2 \theta_3 - \theta_4)$$

or

$$T_L = K_2 \left[(A_2 - A_3) \sin \omega t + (B_2 - B_3) \cos \omega t + \frac{(\tau_1 + \tau_2)}{K_2}\right] \tag{9a}$$

$$T_H = K_4 \left[(n_1 n_2 A_3 - A_4) \sin \omega t + (n_1 n_2 B_3 - B_4) \cos \omega t + \frac{n_1 n_2(\tau_1 + \tau_2)}{K_3}\right] \tag{9b}$$

Torque ripple is calculated from these results and Eq. (1). A computer code was written to facilitate numerical evaluation of torque ripple by evaluating Eqs. (7), (9) and (1), with intermediate steps as necessary.

DATA ACQUISITION AND REDUCTION

As mentioned before, there are two torque sensors in the drive train of the 17 meter turbine; one on the low speed end and the other on the high speed end. In conjunction with these, there are also two anemometers mounted atop the turbine at heights of 27 meters (94 feet) and 34 meters (110 feet). All of the data presented here are based upon anemometry at the 27 meter level. The data flow of the above instruments, along with other telemetry, is fed into a mini-computer that provides data reduction, display, and storage (6).

The turbine was tested at four synchronous rotor speeds; 29.6, 37.0, 45.5, and 52.5 RPM. Both modes of generator coupling (induction only, induction and synchronous) were performed at these speeds. To observe the dependence of $\tilde{T}$ upon drive train stiffness, testing was performed with all the shear sandwich mountings present (stiff drive train) and with half of them removed from the flexible couplings on the low speed end (soft drive train).

Each particular test run had a duration of 15 minutes during which the torque sensors and anemometry were sampled at 0.1 second intervals. The number of permutations of turbine speed, generators, and drive train stiffnesses, coupled with wind availability and other testing priorities, usually allowed one to two test runs per permutation or none at all. The accumulated data were stored on a computer disk.

The output torque of a two bladed Darrieus wind turbine is assumed to be harmonic and was modeled as a cosine function in this paper. A typical example of the raw torque data is shown in Fig. 3 for 37 RPM. A cosine function has the

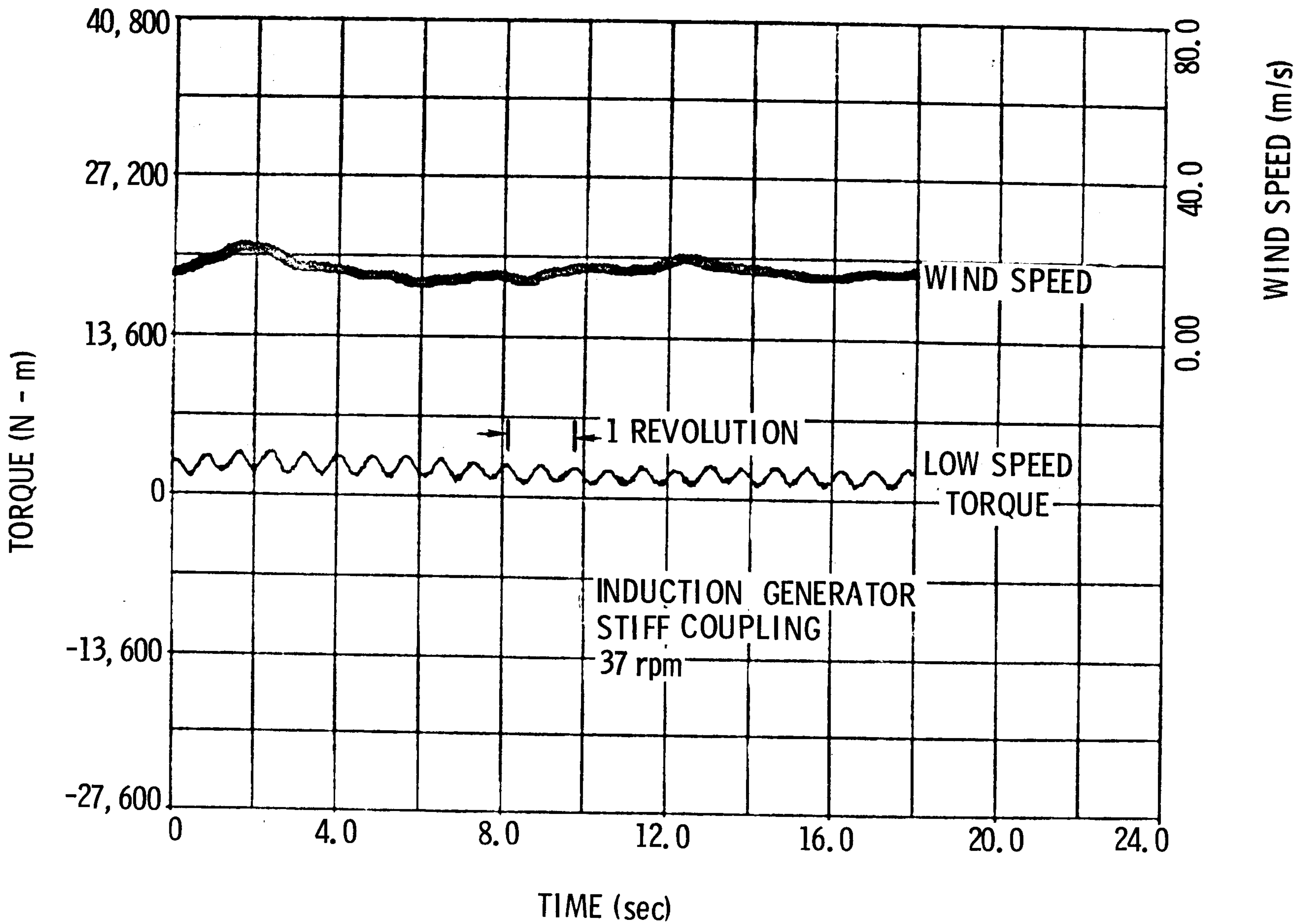

Fig. 3 - Sample of torque data as collected

property that its maximum value can be found by multiplying the root mean square deviation by $\sqrt{2}$ and adding to the mean:

$$T_{max} = \sqrt{2}\, T_{RMS} + T_{mean} \tag{10}$$

$$T_{RMS} = \left[\frac{1}{n} \sum_{i=1}^{n} (y_i - y_{mean})^2\right]^{\frac{1}{2}} \tag{11}$$

where y_i are values of points on the cosine curve located at equal time increments. This equation for the maximum value of a cosine function is substituted into the equation for $\tilde{T}$ giving:

$$\tilde{T} = \frac{T_{max} - T_{mean}}{T_{mean}} = \frac{\sqrt{2}\, T_{RMS}}{T_{mean}} \tag{12}$$

The data reduction method utilized here is based upon the assumption that the mean wind remains steady over five second intervals. Through this assumption, both the turbine rotor torque and the accompanying drive train torque will be harmonic during this period. For each five seconds of data, the average wind velocity, average torque, RMS torque, tip speed ratio, λ, and $\tilde{T}$ from Eq. (12) are calculated. These values of $\tilde{T}$ are grouped according to their corresponding λ and are averaged at the end of the data sampling period. The final output lists λ, the corresponding average $\tilde{T}$ for that λ and the number of five second intervals that went into the calculation of the average $\tilde{T}$.

It is necessary to group $\tilde{T}$ according to λ because the actual aerodynamic torque output of the rotor, which is harmonic, will shift its mean according to λ. Values of λ from 4.0 to 9.0 were used in increments of 1.0. Below $\lambda = 4.0$, the rotor blades begin to stall and the corresponding rotor torque no longer follows a harmonic shape.

The basic assumption of this method of data reduction is that the mean wind velocity was steady over each five second period. By its nature, the wind is seldom steady and will always exhibit some kind of fluctuation. While this method of data reduction is not sensitive to slow velocity fluctuations, it will be sensitive to wind gusting. In addition, any slack in the drive train of the turbine will cause erroneous torque readings. Torsional slack present on the high speed end of the 17 meter turbine is approximately 200°.

In compliance with the basic assumptions of the present theory, approximately 5% of the total data collected were discarded because it was obtained during periods of extreme wind gustiness, or when wind-up of drive train slack was encountered.

CORRELATION OF THEORY AND DATA

Numerical results for torque ripple in the low speed shaft of the DOE/Sandia 17 meter turbine are shown as a function of turbine operating speed in Figs. 4 and 5, with tip speed ratio as a parameter, along with experimental data at four operating speeds. Each data point in the figures represents the average of numerous measurements at the designated operating speed and tip speed ratio. These values of torque ripple are seen by all low speed drive train components, including the transmission. Mean and oscillatory amplitudes of the applied torques, T_{A1} and T_{A2}, were obtained from normalized aerodynamic data (7), and are given in Table II. Normalized data may be used for evaluation of torque ripple by virtue of its definition, Eq. (1).

Each curve has a limiting torque ripple value (as operating speed approaches zero) which is relatively high (above 100%). This value represents the ripple in the applied torques, and is also the value which would be transmitted all the way to the generator, at any operating speed, if the entire turbine and drive train

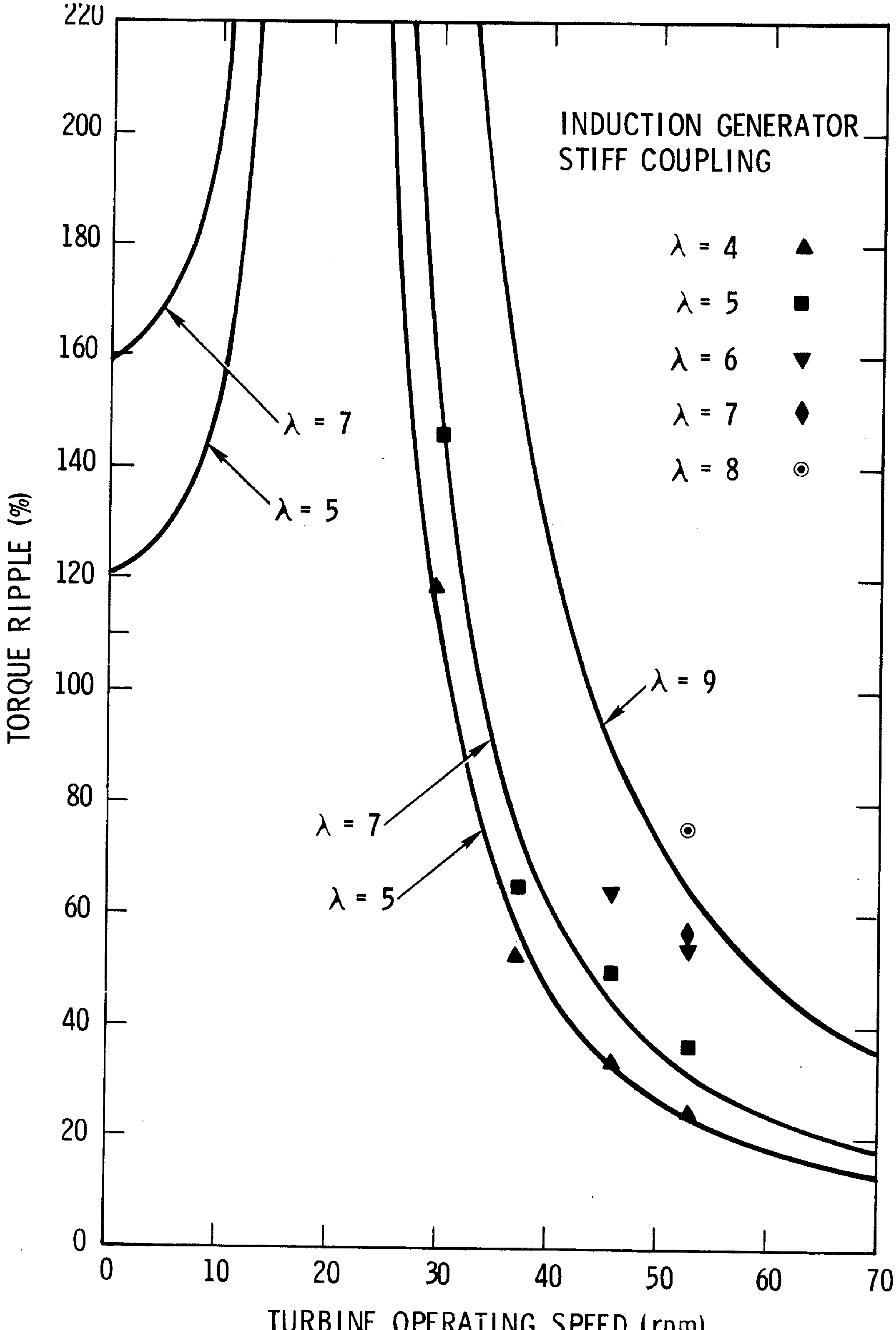

Fig. 4 - Correlation of analytical predictions and experimental data of torque ripple for the stiff drive train

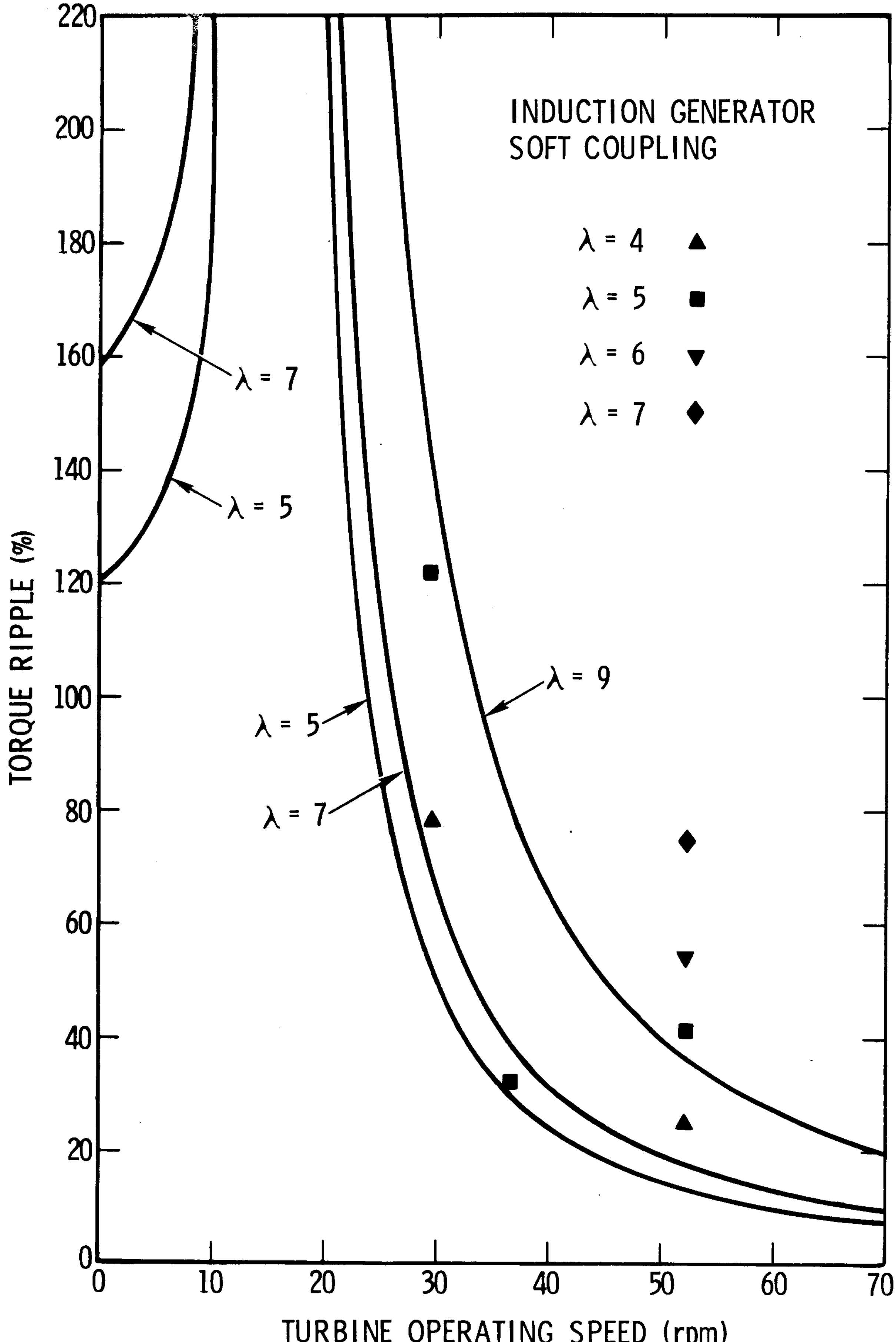

Fig. 5 - Correlation of analytical predictions and experimental data of torque ripple for the soft drive train

TABLE II. Applied Torque Components

λ	5	7	9
$T_1 = T_2$	.274	.307	.383
${}_1 = {}_2$	.226	.193	.117

were rigid and massless. Because of component flexibilities and torsional inertias, torque ripple increases from the initial value as the operating speed of the turbine approaches the first critical drive train frequency. Operating speeds above the first critical frequency bring about significant attenuation of torque ripple. At the first critical frequency, torque ripple remains finite by virtue of the generator dissipation coefficient, D (and other actual losses not account for), however, the ordinate scale of Figs. 4 and 5 was chosen to demonstrate other interesting features of the curves and not peak torque ripple values (clearly to be avoided anyway). Attenuation of torque ripple continues as turbine operating speeds are increased until the next critical drive train frequency is reached. This, too, was beyond the range of an interesting abscissa scale.

Several trends which are visible in the data have been predicted by the analytical model. The predicted attenuation of torque ripple at operation speeds above the first critical has been corroborated by experimental data. Theory and experiment also agree that the attenuation diminishes with increased operating speed. This behavior suggests strongly that a vertical axis wind turbine be operated at a speed well above its first critical drive train frequency in order to minimize torque ripple. Also, torque ripple increases (at an increasing rate) with tip speed ratio for a particular operating speed. The present theory slightly underpredicts the magnitude of these changes with λ. It tends to overpredict torque ripple at low tip speed ratios and underpredicts it at high tip speed ratios. A plausible explanation for this would be inaccuracies in the basic aerodynamic data used to produce Table II, and poorly satisfied assumptions (see Analysis).

The synchronous operating speed of a turbine is likely to be selected by aerodynamic performance criteria, accompanied by design efforts which attempt to select and manipulate structural properties of the turbine in such a way that static and dynamic problems are avoided (8). For example, to increase the spread between the operating speed of a turbine and the first critical drive train frequency (in order to minimize torque ripple) an attempt should be made to reduce the drive train frequency before compromising performance by increasing the operating speed. A reduction of the first critical drive train frequency shifts the entire torque ripple curve to the left, thereby reducing ripple at the selected operating speed. This can be accomplished by reducing the torsional rigidity of the drive train. As mentioned previously, the DOE/Sandia 17 meter turbine has features which allow torsional rigidity to be reduced easily so that this effect can be demonstrated. Results in Fig. 4 are for the original drive train stiffness, and those in Fig. 5 are for approximately a 43% reduction in the stiffness of the low speed portion of the drive train. Two changes take place. First, torque ripple is reduced over operating speeds above the first critical frequency; and second, the variation in torque ripple with λ at a particular operating speed is reduced. These changes are predicted theoretically and observed experimentally as illustrated in Figs. 4 and 5.

Another part of this investigation included a look at the differences in torque ripple between operation with an induction generator and operation with a synchronous/induction generator combination. The 17 meter turbine generator arrangement required only that a torsional stiffness constant, k, be added to the induction generator model, Fig. 2, in order to characterize the synchronous/induction generator combination analytically. This change had very little effect on the numerical results (it shifted $\widetilde{T}$ curves slightly to the left), so additional theoretical curves are not presented for the synchronous/induction generator combination. However, experimental data are shown in Figs. 6 and 7 where torque ripple results for the synchronous/induction generator operation are compared to those for the induction generator alone. The only observable difference between

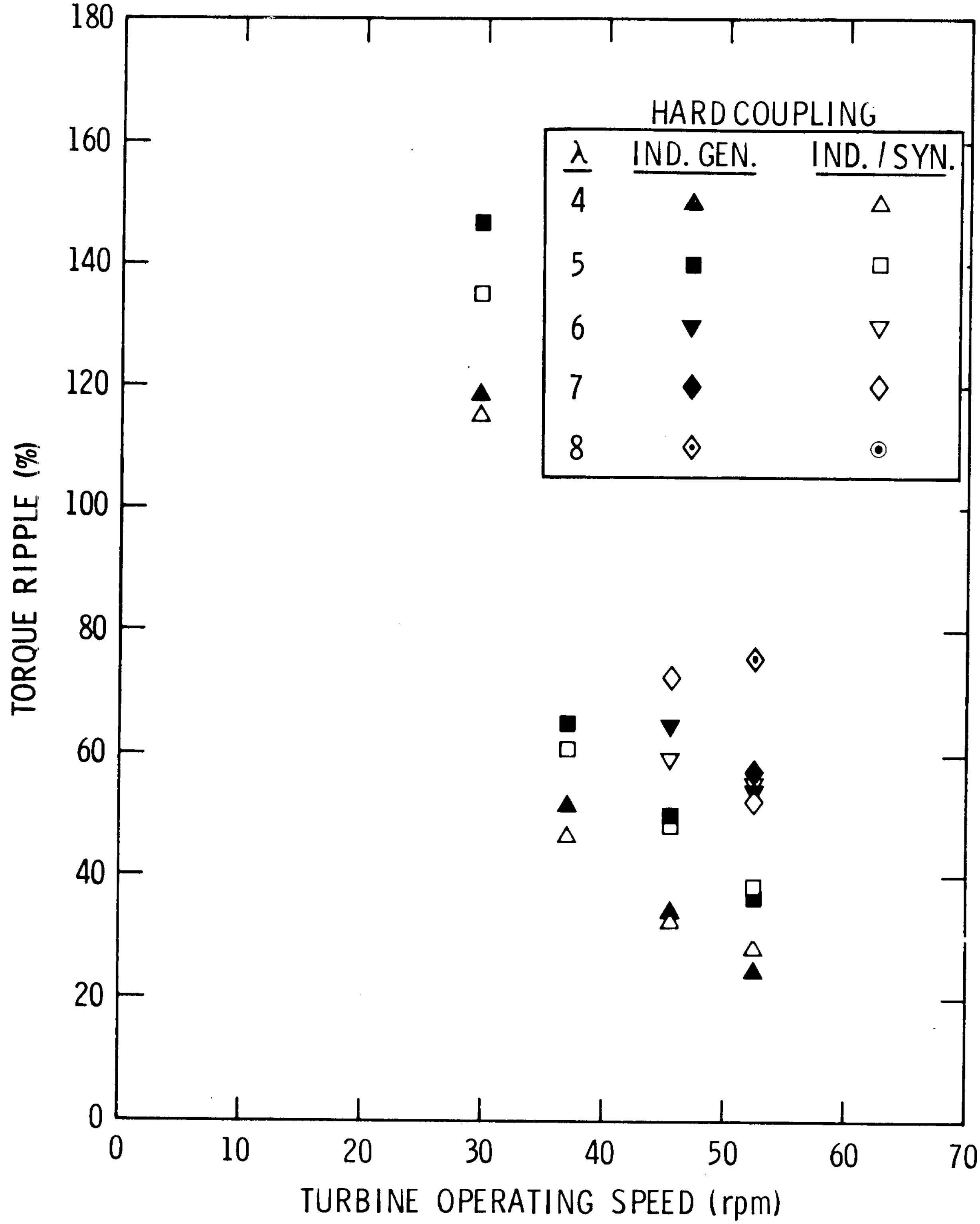

Fig. 6 - Experimental data comparison of torque ripple with the induction generator and induction/synchronous generator combination (stiff drive train)

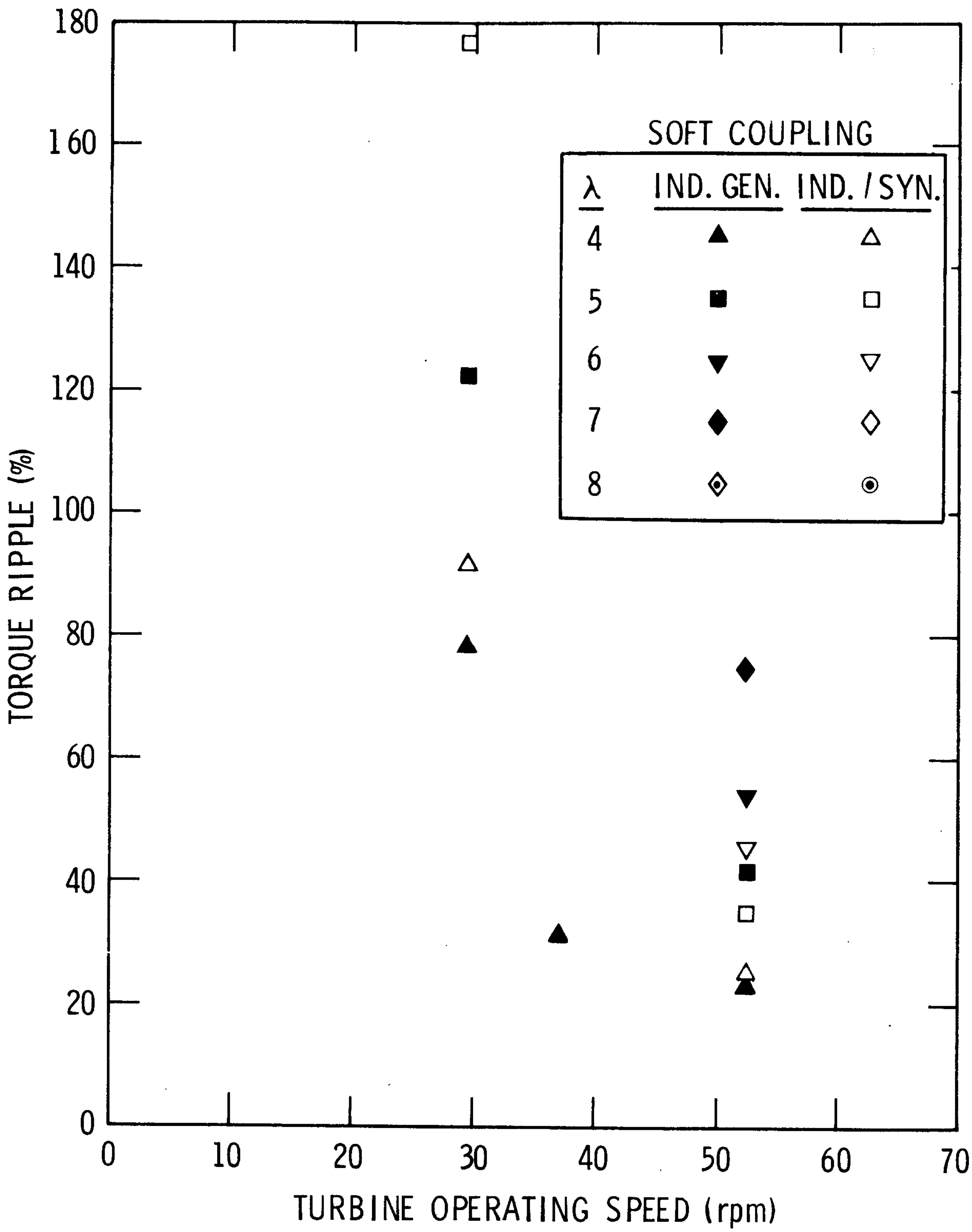

Fig. 7 - Experimental data comparison of torque ripple with the induction generator and induction/synchronous generator combination (soft drive train)

the two sets of data is that the spread in torque ripple with λ at a particular operating speed is generally less for the synchronous generator than for the induction generator. This behavior is consistent with that occurring whenever drive train torsional rigidity is reduced, as with the addition of the synchronous generator stiffness, k.

Thus far, results have been presented for torque ripple in the low speed shaft only. Data were also obtained at the high speed shaft where torque ripple was found to be consistently higher than in the low speed shaft. This torque ripple magnification is due to power losses which occur between the high and low speed shafts, principally in the transmission. It is seen by all high speed drive train components including the generator. To a first approximation, the losses produce a uniform reduction in torque. This causes the mean and peak torque values to be reduced by the same amount, thereby reducing the mean value without changing the mean-to-peak value of torque (see Eq. 1). The net effect is an increase in torque ripple downstream of the power losses. This magnification can be shown to be of the form

$$M_T = \frac{1}{1 - f} \tag{10}$$

where f is the ratio of the power lost to the mean power before losses occur. High speed torque ripple can be estimated, therefore, from low speed values by

$$\tilde{T}_H = M_T \tilde{T}_L \tag{11}$$

Alternately, if high and low speed torque ripple is known, it can be used with Eqs. (10) and (11) to estimate power losses between the two data acquisition locations. High speed torque ripple data will be presented under separate cover where space will allow proper reconciliation of the data with power loss measurements.

DISCUSSION AND CONCLUSIONS

Three methods of reducing torque ripple in wind turbines are available, and are equally effective for both the horizontal axis and the vertical axis type. They are: a reduction of torsional rigidity of the drive train, a reduction of power losses and the addition (or systematic location) of rotational inertia along the drive train. In the original design of a turbine, it is advisable to make the drive train (below the turbine) as compliant as practical in order to reduce torque ripple at turbine operating speeds. If it is found that the drive train is still too stiff, the location for placement of additional compliance must be selected. It has been stated (9) that reducing high speed shaft stiffness will reduce torque ripple, and indeed it will. However, it is not necessarily the most effective location for this reduction. In calculating an equivalent torsional stiffness for the entire drive train, with respect to the low speed end, high speed stiffness values are multiplied by the gear ratio squared, thus generally making them quite large compared to low speed values. The equivalent stiffness of the entire drive train will be dominated by its softest components, and changes in these components will produce the greatest changes in the equivalent stiffness. Therefore, the location where it is easiest to achieve added torsional compliance is generally the low speed end of the drive train, immediately below the rotor. Also see (1).

It has been shown (above) how power losses in the drive train can magnify torque ripple downstream from the turbine. There are now two incentives for minimizing power losses. First is the obvious and well known effect of improving operating efficiency of the turbine, and second is the reduction of downstream torque ripple.

The third method of reducing torque ripple is an alternate (or companion) means of reducing the first critical drive train frequency. Arguments which guided placement of torsional compliance to the low speed end are repeated for placement of added (or relocated) torsional inertia. However, since inertia at the high speed end (even when corrected to the low speed end) is usually lower than at the low speed end (rotor inertia), the most effective location for torsional inertia is the high speed end of the drive train. Simply adding mass to the high speed shafts should be considered only after careful evaluation of the possibility of relocating other drive train components already present. For example, brake discs located at the low speed end should be placed at the high speed end of the drive train. One should note, however, that heat dissipation and braking torque requirements will be different at the high speed end than at the low speed end.

A synchronously operating Darrieus wind turbine experiences its maximum power (and mean torque) output at a tip speed ratio, λ, of about 2.5 to 4 (5). As λ increases, the power and mean torque diminish, and the torque ripple, Figs. 4 and 5, increases. For example, at an operating speed of 45.5 RPM, torque ripple predictions are 30%, 45% and 80% for $\lambda = 5$, 7 and 9, respectively. These torque ripple values give the magnitude of the oscillatory torque as a percent of the mean torque at that λ. If the torque ripple values are expressed in terms of the <u>maximum, or rated torque for that operating speed</u>, they become 11%, 5% and 1.5%, respectively. Therefore, torque ripple based on <u>rated torque</u> is maximum at peak power ($\lambda \simeq 2.5$ to 4), and is considerably lower than what might be concluded by referring to Figs. 4 and 5 directly. It is this value which must be used when considering the impact of torque ripple on design.

This investigation has permitted an initial understanding of the torque ripple phenomenon, and an evaluation of its magnitude and possibilities for controlling it. Topics for further investigation include evaluation of torque ripple for a three bladed vertical axis wind turbine, calculation of other drive train frequencies (although at present they appear to be well above turbine operating speeds), effects of blade dynamics, effects of variable winds, effects of drive train slack, pure synchronous operation and further evaluation of torque ripple magnification due to power losses.

The present theory has yielded the following conclusions:

1. The wind turbine operating speed should be located well above the first critical drive train frequency.

2. Torque ripple increases with tip speed ratio at a particular operating speed.

3. There is a magnification of torque ripple downstream of the rotor due to power losses in the drive train.

4. Torque ripple data can be used to measure power losses.

5. The drive train, below the rotor, should be made as compliant as practical. If additional compliance is required, it is generally most effective when placed in the low speed end.

6. Added or relocated rotational inertia is generally most effective in reducing torque ripple when it is placed in the high speed end.

It appears that the measured and predicted values of torque ripple presented in this report are sufficiently large to pose a potential problem. Torque ripple should be reduced as much as possible in subsequent turbine designs by the methods discussed above, however, exactly what constitutes an acceptable level is not known at the present time.

ACKNOWLEDGMENT

The authors gratefully acknowledge the assistance of several Sandia Laboratories' personnel; R. E. Akins for his assistance in suggestions for data reduction, W. N. Sullivan and E. G. Kadlec for helpful discussions, and P. C. Klimas for calculation of aerodynamic loads.

REFERENCES

1. L. P. Mirandy, "Rotor/Generator Isolation for Wind Turbines," Journal of Energy, Vol. 1, No. 3, May-June 1977.
2. B. F. Blackwell, L. V. Feltz, "Wind Energy - A Revitalized Pursuit," Sandia Laboratories Report No. SAND75-0166, March 1975.
3. B. F. Blackwell, W. N. Sullivan, R. C. Reuter, J. F. Banas, "Engineering Development Status of the Darrieus Wind Turbine," Journal of Energy, Vol. 1, No. 1, Jan.-Feb. 1977.
4. R. C. Reuter, "Tower Analysis," ERDA Vertical Axis Wind Turbine Technology Workshop, Albuquerque, NM, May 1976.
5. J. F. Banas, W. N. Sullivan, Editors, "Sandia Vertical-Axis Wind Turbine Program Technical Quarterly Report," Sandia Laboratories Report No. SAND76-0036, April 1976.
6. B. Stiefeld, "Wind Turbine Data Acquisition and Analysis System," Sandia Laboratories Report No. SAND77-1164, December 1977.
7. P. C. Klimas, Sandia Laboratories, private communication.
8. J. F. Banas, W. N. Sullivan, "Engineering of Wind Energy Systems," Sandia Laboratories Report No. SAND75-0530, January 1975.
9. T. L. Sullivan, D. R. Miller, D. A. Spera, "Drive Train Normal Modes Analysis for the ERDA/NASA 100-Kilowatt Wind Turbine Generator," NASA Report No. NASA TM 73718, July 1977.

DISTRIBUTION:

TID-4500-R66 UC-60 (283)

Aero Engineering Department (2)
Wichita State University
Wichita, KS 67208
Attn: M. Snyder
W. Wentz

Dr. Daniel K. Ai
Senior Scientific Associate
Alcoa Laboratories
Aluminum Company of America
Alcoa Center, PA 15069

Mr. Robert B. Allen
General Manager
Dynergy Corporation
P.O. Box 428
1269 Union Avenue
Laconia, NH 03246
Alcoa Center, PA 15069

American Wind Energy Association
54468 CR31
Bristol, IN 46507

E. E. Anderson
South Dakota School of Mines
and Technology
Department of Mechanical Engineering
Rapid City, SD 57701

P. Bailey
P.O. Box 3
Kodiak, AK 99615

F. K. Bechtel
Washington State University
Department of Electrical Engineering
College of Engineering
Pullman, WA 99163

M. E. Beecher
Arizona State University
Solar Energy Collection
University Library
Tempe, AZ 85281

K. Bergey
University of Oklahoma
Aero Engineering Department
Norman, OK 73069

Dr. B. F. Blackwell
Department of Mechanical Engineering
Lousisiana Tech University
Ruston, LA 71270

Dr. P. H. Bottelberghs
Chemical Conversion and Energy Storage
Landelijke Stuurgroep Energie Onderzoek
Dutch National Steering Group for
Energy Research
Laan van Vollenhove 3225
Zeist
THE NETHERLANDS

Robert Brulle
McDonnell-Douglas
P.O. Box 516
Department 241, Building 32
St. Louis, MO 63166

R. Camerero
Faculty of Applied Science
University of Sherbrooke
Sherbrooke, Quebec
CANADA J1K 2R1

A. N. L. Chiu
University of Hawaii
Wind Engineering Research Digest
Spalding Hall 357
Honolulu, HI 96822

Dr. R. N. Clark
USDA, Agricultural Research Service
Southwest Great Plains Research Center
Bushland, TX 79012

U. A. Coty
Lockheed California Co.
Box 551-63A1
Burbank, CA 91520

Arthur G. Craig
Alcoa Mill Products
Alcoa Center, PA 15069

DOE/ALO (3)
Albuquerque, NM 87115
Attn: D. K. Nowlin
W. P. Grace
D. W. King

DOE Headquarters (20)
Washington, DC 20545
Attn: L. V. Divone, Chief
Wind Energy Conversion Branch
D. D. Teague
Wind Energy Conversion Branch

Prof. A. V. da Rosa
C.P. 1.170 (UNICAMP)
13.100 Campinas, S.P.
BRAZIL

C. W. Dodd
School of Engineering
Southern Illinois University
Carbondale, IL 62901

D. P. Dougan
Hamilton Standard
1730 NASA Boulevard
Room 207
Houston, TX 77058

J. B. Dragt
Nederlands Energy Research Foundation (E.C.N.)
Physics Department
Westerduinweg 3 Patten (nh)
THE NETHERLANDS

Electric Power Research Institute
3412 Hillview Avenue
Palo Alto, CA 94304
Attn: P. Bos

William J. Ewing, President
Research Dynamics Associates
P.O. Box 211
Menlo Park, CA 94025

J. Fischer
F. L. Smidth & Company A/S
Vigerslevalle 77
2500 Valby, DENMARK

Robert E. Fisher
Environmental Protection Specialist
Department of Environmental Resources
736 West Fourth Street
Williamsport, PA 17701

James D. Fock, Jr.
Department of Aerospace Engineering Sciences
University of Colorado
Boulder, CO 80309

W. F. Foshag
Aerophysics Company
3500 Connecticut Avenue NW
Washington, DC 20008

Albert Fritzsche
Dornier System GmbH
Postfach 1360
7990 Friedrichshafen
WEST GERMANY

W. W. Garth, IV
Tyler & Reynolds & Craig
One Boston Place
Boston, MA

E. Gilmore
Amarillo College
Amarillo, TX 79100

Mr. Richard Gorman
TRW Energy Systems
7600 Colshire Drive
McLean, VA 22101

Professor N. D. Ham
Massachusetts Institute of Technology
77 Massachusetts Avenue
Cambridge, MA 02139

Sam Hansen
DOE/DSE
20 Massachusetts Avenue
Washington, DC 20545

Donald M. Hardy
SERI
1536 Cole Blvd.
Golden, CO 80401

W. L. Harris
Aero/Astro Deprtment
Massachusetts Institute of Technology
Cambridge, MA 02139

Terry Healy (2)
Rocky Flats Plant
P.O. Box 464
Golden, CO 80401

P. W. Hill
Allegany Ballistics Laboratory
Hercules, Inc.
P.O. Box 210
Cumberland, MD 21502

Sven Hugosson
Box 21048
S. 100 31 Stockholm 21
SWEDEN

O. Igra
Department of Mechanical Engineering
Ben-Gurion University of the Negev
Beer-Sheva, ISRAEL

JBF Scientific Corportion
2 Jewel Drive
Wilmington, MA 01887
Attn: E. E. Johanson

J. P. Johnston
Stanford University
Department of Mechanical Engineering
Stanford, CA 94305

Kaman Aerospace Corporation
Old Windsor Road
Bloomfield, CT 06002
Attn: W. Batesol

O. Krauss
Michigan State University
Division of Engineering Research
East Lansing, MI 48824

S. M. Lambert, Manager
Energy Economics and Forecasting
  Planning and Economics
Shell Oil Company
P.O. Box 2463
Houston, TX 77001

Lawrence Livermore Laboratory
P.O. Box 808 L-340
Livermore, CA 94550
Attn: D. W. Dorn

M. Lechner
Public Service Company of New Mexico
P.O. Box 2267
Albuquerque, NM 87103

J. Lerner
State Energy Commission
Research and Development Division
1111 Howe Avenue
Sacramento, CA 95825

L. Liljdahl
Building 303
Agriculture Research Center
USDA
Beltsville, MD 20705

P. B. S. Lissaman
Aeroenvironment, Inc.
660 South Arroyo Parkway
Pasadena, CA 91105

Olle Ljungstrom
Swedish Board for Technology Development
FACK
S-100 72 Stockholm 43, SWEDEN

Los Alamos Scientific Laboratories
P.O. Box 1663
Los Alamos, NM 87544
Attn: J. D. Balcomb Q-DO-T
Library

L. H. J. Maile
48 York Mills Rd.
Willowdale, Ontario
CANADA M2P 1B4

Frank Matanzo
Dardalen Associates
15110 Frederick Road
Woodbine, MD 21797

James Meiggs
Kaman Sciences Corporation
P.O. Box 7463
Colorado Springs, CO 80933

R. N. Meroney
Colorado State University
Department of Civil Engineering
Fort Collins, CO 80521

G. N. Monsson
Department of Economic Planning and Development
Barrett Building
Cheyenne, WY 82002

Don Myrick
105 Skipper Avenue
Ft. Walton Beach, FL 32548

NASA
Langley Research Center
Hampton, VA 23665
Attn: R. Muraca, MS317

NASA Lewis Research Center (2)
2100 Brookpark Road
Cleveland, OH 44135
Attn: J. Savino, MS 509-201
R. L. Thomas
W. Robbins

V. Nelson
West Texas State University
Department of Physics
P.O. Box 248
Canyon, TX 79016

Oklahoma State University (2)
Stillwater, OK 76074
Attn: W. L. Hughes
EE Department
D. K. McLaughlin
ME Department

Oregon State University (2)
Corvallis, OR 97331
Attn: R. Wilson
ME Department
R. W. Thresher
ME Department

H. H. Paalman
Dow Chemical USA
Research Center
2800 Mitchell Drive
Walnut Creek, CA 94598

J. Park
Helion
P.O. Box 4301
Sylmar, CA 91342

R. A. Parmelee
Northwestern University
Department of Civil Engineering
Evanston, IL 60201

B. Maribo Pedersen
Department of Fluid Mechanics
Building 404, DTH
2800 Lyngby
DENMARK

A. Robb
Memorial University of Newfoundland
Faculty of Engineering and Applied Sciences
St. John's Newfoundland
CANADA A1C 5S7

Tim P. Romero
P.O. Box 2806
Las Vegas, NM 87701

A. V. da Rosa
Stanford Electronic Laboratories
Radio Science Laboratory
Stanford, CA 94305

H. Sevier
Rocket and Space Division
Bristol Aerospace Ltd.
P.O. Box 874
Winnipeg, Manitoba
CANADA R3C 2S4

P. N. Shankar
Aerodynamics Division
National Aeronautical Laboratory
Bangalore 560017
INDIA

D. G. Shepherd
Cornell University
Sibley School of Mechanical and
Aerospace Engineering
Ithaca, NY 14853

Dr. Fred Smith
Mechanical Engineering Department Head
Colorado State University
Ft. Collins, CO 80521

Leo H. Soderholm
Iowa State University
Agricultural Engineering, Room 213
Ames, IA 50010

Southwest Research Institute (2)
P.O. Drawer 28501
San Antonio, TX 78284
Attn: W. L. Donaldson, Senior Vice President
R. K. Swanson

Dale T. Stjernholm, P.E.
Mechanical Design Engineer
Morey/Stjernholm and Associates
1050 Magnolia Street
Colorado Springs, CO 80907

E. S. Takle
Iowa State University
Climatology and Meteorology
312 Curtiss Hall
Ames, IA 50010

R. J. Templin (3)
Low Speed Aerodynamics Section
NRC-National Aeronautical Establishment
Ottawa 7, Ontario
CANADA K1A OR6

Texas Tech University (3)
P.O. Box 4289
Lubbock, TX 79409
Attn: K. C. Mehta, CE Department
J. Strickland, ME Department
J. Lawrence, ME Department

Fred Thompson
Atari, Inc.
155 Moffett Park Drive
Sunnyvale, CA 94086

United Engineers and Constructors, Inc.
Advanced Engineering Department
30 South 17th Street
Philadelphia, PA 19101
Attn: A. J. Karalis

United Nations Environment Program
485 Lexington Avenue
New York, NY 10017
Attn: I. H. Usmani

University of New Mexico (2)
Albuquerque, NM 87106
Attn: K. T. Feldman
Energy Research Center
V. Sloglund
ME Department

A. G. Vacroux
Illinois Institute of Technology
Department of Electrical Engineering
3300 South Federal
Chicago, IL 60616

P. N. Vosburgh, Development Manager
Alcoa Allied Products
Alcoa Center, PA 15069

Otto de Vries
National Aerospace Laboratory
Anthony Fokkerweg 2
Amsterdam 1017
THE NETHERLANDS

R. Walters
West Virginia University
Department of Aero Engineering
1062 Kountz Avenue
Morgantown, WV 26505

E. J. Warchol
Bonneville Power Administration
P.O. Box 3621
Portland, OR 97225

R. G. Watts
Tulane University
Department of Mechanical Engineering
New Orleans, LA 70018

T. Wentink, Jr.
University of Alaska
Geophysical Institute
Fairbanks, AK 99701

West Texas State University
Government Depository Library
Number 613
Canyon, TX 79015

C. Wood
Dominion Aluminum Fabricating Ltd.
3570 Hawkestone Road
Mississauga, Ontario
CANADA L5C 2V8

1000 G. A. Fowler
1200 L. D. Smith
1260 K. J. Touryan
1280 T. B. Lane
1281 S. W. Key
1282 T. G. Priddy
1284 R. T. Othmer
1284 R. C. Reuter, Jr. (20)
1300 D. B. Shuster
1320 M. M. Newsom
1324 E. C. Rightley
1324 L. V. Feltz
1330 R. C. Maydew
1331 H. R. Vaughn
1332 C. W. Peterson
1333 S. McAlees, Jr.
1333 R. E. Sheldahl
1334 D. D. McBride
1335 W. R. Barton
1336 J. K. Cole
3161 J. E. Mitchell (50)
3161 P. S. Wilson
5333 R. E. Akins
5333 J. W. Reed
5700 J. H. Scott
5710 G. E. Brandvold
5715 R. H. Braasch (200)
5715 E. G. Kadlec
5715 B. Stiefeld
5715 W. N. Sullivan
5715 M. H. Worstell
8266 E. A. Aas
3141 C. A. Pepmueller (Actg) (5)
3151 W. L. Garner (3)
For DOE/TIC (Unlimited Release)
DOE/TIC (25)
(R. P. Campbell, 3172-3)

Reprinted January 1980

Reprinted March 1982